

Effect of Ni Substitution on Structural and Magnetic Properties of Mn-Zn Ferrite Nanoparticles

F. A. Ahmed · L. N. Singh

Department of Physics, Dr. Babasaheb Ambedkar Technological University, Lonere, Raigad-402103, Maharashtra, India.

ABSTRACT

The nickel substituted Mn-Zn spinel ferrite system has been prepared by sol-gel method. The XRD patterns confirm the synthesis of single phase ferrite nanoparticles for all the samples. The lattice parameter and the distance between magnetic ions for each A-site and B-site were found to decrease with increasing nickel content. The crystallite size of the samples was determined from XRD and found in the range of 29-37nm. The B-H loop parameters, g-value, linewidth ΔH_{pp} , resonance field have been investigated at room temperature. It has also been observed that saturation magnetization increases up to $x=0.1$ and then decreases. The EPR study reveals the super paramagnetic nature of the materials.

© 2018 JMSSE and Science IN. All rights reserved

ARTICLE HISTORY

Received 26-04-2018
Revised 03-07-2018
Accepted 05-07-2018
Published 04-10-2018

KEYWORDS

Spinel ferrite; Nanoparticle; sol-gel method; Saturation magnetization; SEM

Introduction

The nanoparticles with unique magnetic properties and their pledging technological applications have attracted considerable attention in the recent years [1]. Soft ferromagnetic oxides are of great importance as high-frequency magnetic materials. The general formula for these compounds is MFe_2O_4 , where M is a divalent metal ion such as $Fe^{2+}, Ni^{2+}, Mg^{2+}, Mn^{2+}, Zn^{2+}, Cu^{2+}$ etc. or a mixture of these ions [2]. Through the choice of various divalent cations in the ferrites, the magnetic properties can be tuned and customized according to technological applications [3].

Mn-Zn ferrite nanoparticles have a wide range of magnetic applications such as recording heads, transformer cores, and noise filters etc. because of their superior magnetic properties such as high saturation magnetization and high initial permeability [4, 5]. Mn-Zn ferrites are usually limited to frequencies <500 kHz due to their relatively low resistivities ($0.02-20 \Omega m$) [6], and in consequence, these ferrite nanoparticles are not suitable for magnetic applications at higher frequencies due to high eddy current losses. Ni-Zn ferrite nanoparticles have many attractive properties and a wide range of technological applications such as low and high-frequency transformer cores, antenna rods and microwave devices due to their low eddy currents and dielectric losses, inferior magnetic properties at higher frequencies limit their use [7]. Through the suitable combination of Mn-Zn and Ni-Zn ferrite nanoparticles, a material can be achieved with not only high resistivity but also appreciative magnetic properties. This is suitable for magnetic applications at higher frequencies with minimum power losses due to eddy currents [5, 8]. Amrendra K. Singh et al. reported that Mn-Ni-Zn ferrites have a high resistivity in the range of $10^5-10^7 \Omega cm$ as well as high initial permeability in the range of 50-290 [9]. C. O. Ehi-Eromosele et al. reported that Ni-Zn nanoferrites synthesized by the low-temperature auto-combustion method have saturation magnetization in the range of 25-36 emu/g [10]. B. Jeyadevan et al. have reported Mn-Zn ferrite nanoparticles with saturation magnetization in the range of 37-50 emu/g [11]. N. T. Lan et al. observed that

$Mn_{1-x}Zn_xFe_2O_4$ ($x=0, 0.1, 0.3, 0.5, 0.7$) ferrite nanoparticles prepared by using co-precipitation have saturation magnetization in the range of 11.7-25.0 emu/g [12].

The synthesis method plays a revealing role in the properties of the ferrite nanoparticles because properties of nanoparticles depend on shape and size. Several methods of preparation, such as hydrothermal process, the ball milling methods, the sol-gel method and the micro-emulsion methods have been developed to obtain ferrite nanoparticles [13]. The sol-gel method has become very attractive recently for the preparation of nanoferrites due to the high chemical homogeneity, low processing temperatures and the possibility of controlling the size and morphology of the particles [14]. In the present work $Mn_{0.5-x}Ni_xZn_{0.5}Fe_2O_4$ ($x=0.0, 0.1, 0.2, 0.3$) ferrite nanoparticles have been synthesized by sol-gel method and we reported the structural and magnetic properties.

Experimental

Materials & Methods

Nanoparticles of $Mn_{0.5-x}Ni_xZn_{0.5}Fe_2O_4$ ($x=0.0, 0.1, 0.2, 0.3$) have been prepared by a sol-gel method using analytical grade metal chlorides as starting materials. In this process, for sample $x=0$, 1.7158 g of manganese chloride, 1.4447 g of zinc chloride, 6.8772 g of iron chloride, 12.2186 g of citric acid and 24.4373 g of ethylene glycol were used. In a similar way for the samples $x=0.1, 0.2$ and 0.3 , the stoichiometric amounts of metal chlorides, citric acid and ethylene glycol were used. The metal chlorides were dissolved together in a minimum amount (100 ml) of distilled water to get a clear solution. The mixed solution was kept on a hot plate with continuous stirring. The pH of the solution was adjusted between 6 and 7. During heating, we add citric acid (The molar ratio of metal chlorides to citric acid was taken as 1:3) which removes the insoluble residue, ethylene glycol has been also added in the mixture for homogeneity. During evaporation, the solution becomes viscous and finally formed a very viscous brown gel. The gel was then dried in an oven at $250^\circ C$ for 12 hours, and then it is crushed into fine powder form. The as-prepared powder then annealed at $800^\circ C$ for 2 hours and sintered at

1000°C for half an hour. The obtained materials were characterized by X-ray diffraction (XRD) using Bruker Diffractometer with Cu K α radiation source at room temperature and collected the data for every 0.017 $^\circ$ in the angle range 20-90 $^\circ$ of 2 θ . The magnetization measurements were done at room temperature up to a maximum field of 2Tesla, using Vibrational Sample Magnetometer (VSM). Electron Spin Resonance (ESR) spectra were taken by using an X-band Varian's E-112 ESR spectrometer. SEM images were recorded by using Hitachi E-1010 type Scanning Electron Microscope.

Results and Discussion

XRD and SEM Study

The XRD patterns of the samples are shown in Fig. 1, which confirmed the formation of cubic spinel structure and showing that all the samples are formed in pure phase, as indexed by using JCPDS. The diffraction peaks consist of (220), (311), (222), (400), (422), (511), (440), (531) and (622) planes as shown in Fig. 1. The broad XRD peaks are an indication of reduced particle size of the as-prepared material. In addition to the ferrite peaks, impurities peaks correspond to α -Fe $_2$ O $_3$ have been observed in the XRD patterns of the samples. Probably at increased annealing temperature Fe gets converted into its oxide and the extra peaks are due to the formation of α -Fe $_2$ O $_3$ [14]. The morphology of powder shown in Fig. 2 is porous and agglomerated. This morphology is like that reported by Gholam Reza Mershekari et al. [28]. The fluffy nature and voids in the sol-gel prepared powder are due to large amount of gases evolved during the reaction.

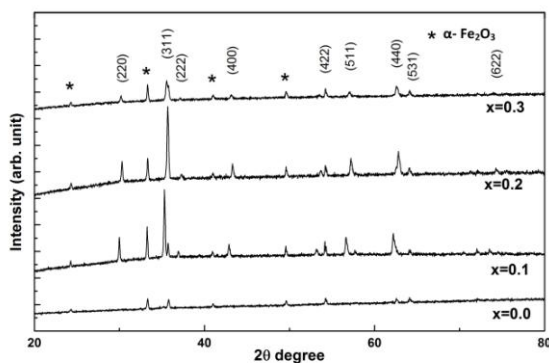


Figure 1: XRD Patterns for Mn $_{0.5-x}$ Ni $_x$ Zn $_{0.5}$ Fe $_2$ O $_4$ (x=0.0, 0.1, 0.2, 0.3)

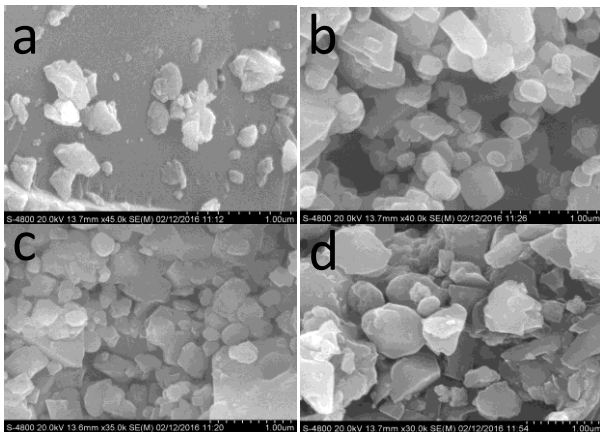


Figure 2: SEM images of Mn $_{0.5-x}$ Ni $_x$ Zn $_{0.5}$ Fe $_2$ O $_4$ ferrite nanoparticles, (a) x=0.0, (b) x=0.1, (c) x=0.2, (d) x=0.3

The average crystallite size (D) has been calculated by using Scherrer formula [15].

$$D = \frac{k\lambda}{\beta \cos \theta} \quad (1)$$

Where k is constant, related to the crystallite shape, normally taken as 0.9 [16], λ is the wavelength of X-ray, β is the full width at half maximum (FWHM) of XRD peak and θ is the Bragg angle for the actual peak.

The lattice parameter (a) has been calculated by using the relation [17].

$$a = d_{hkl} \sqrt{h^2 + k^2 + l^2} \quad (2)$$

Where d_{hkl} is the interplanar separation and h,k,l are Miller indices of the plane.

The XRD density (ρ_x) has been calculated according to the relation [18]

$$\rho_x = \frac{8M}{Na^3} \quad (3)$$

Where 'N' is the Avogadro's number, 'M' is the molecular weight of the sample and 'a' is the lattice constant.

The crystallite size has been calculated from the XRD line width of the (311) peak using equation (1). The values of structural parameters are listed in Table 1.

Table 1: Observed and reported structural parameters of Mn $_{0.5-x}$ Ni $_x$ Zn $_{0.5}$ Fe $_2$ O $_4$ (x=0.0, 0.1, 0.2, 0.3)

Ni Conte nt (x)	Crystallite size (nm)		Lattice Parameter (Å)		Crystallite Density (g/cc)		L _A (Å)		L _B (Å)	
	Obs.	Rep. [40]	Obs.	Rep. [20]	Obs.	Rep. [18]	Obs.	Rep.	Obs.	Rep.
0.0	34.58	14	8.425	8.401	5.258	5.236	3.648	-	2.978	-
0.1	31.94	13.5	8.414	8.390	5.285	5.272	3.643	-	2.974	-
0.2	29.25	14	8.355	8.374	5.407	5.311	3.618	-	2.954	-
0.3	36.48	15.2	8.337	8.368	5.451	5.350	3.610	-	2.948	-

For the unsubstituted sample, 80% of manganese ions occupy the tetrahedral (A-site) position, while the remaining, 20% occupy the octahedral (B-site) position. Zinc and nickel ions prefer to occupy the tetrahedral (A-site) and octahedral (B-site) respectively, while iron ions occupy both tetrahedral (A-site) and octahedral (B-site), it prefers the octahedral (B-site) [19]. It has been observed that both crystallite size and lattice parameter decrease as an increase in nickel ion substitution. This can be explained on the basis of the relative ionic radius. The ionic radius (0.82Å) of Mn $^{2+}$ ions is larger than the ionic radius (0.69Å) of the Ni $^{2+}$ ion. Due to the replacement of smaller Ni $^{2+}$ ions for larger Mn $^{2+}$ ions in the lattice, the unit cell contracts while preserving the cubic symmetry. Though the crystallite size of the sample is found to be minimum with nickel substitution x=0.2. For substitution x=0.3, a significant fraction of Mn $^{2+}$ and Zn $^{2+}$ occupies the B-sites and forces Fe $^{3+}$ to the A-sites against their chemical preferences. The ionic radius (0.69Å) of Ni $^{2+}$ ions is larger than the ionic radius (0.64Å) of Fe $^{3+}$ ions. Due to the replacement of Ni $^{2+}$ ions for Fe $^{3+}$ ions in the sample, the unit cell expands while preserving the cubic symmetry and hence crystallite size increases.

The crystallite sizes and lattice parameters are decreased with increasing Ni substitution, as shown in Fig. 3 and 4. The values of lattice parameters have been observed in the range 8.414 Å to 8.337 Å, are in good agreement with those of C. Venkataraju et al. [20], S. G. Dahotre et al. [21]. The XRD density increases with increase in Ni content and

decrease in Mn content. This increase in XRD density (ρ_x) is a direct effect of the lattice parameter. The effect of the Mn²⁺ concentrations on the microstructure of ferrites has been reported by M. F. Yan and D. Johnson [22].

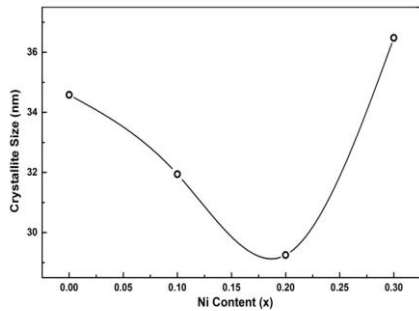


Figure 3: Variation of Crystallite size with Ni content

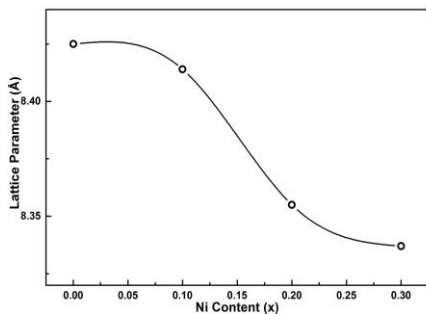


Figure 4: Variation of Lattice Parameter with Ni content

A. Globus et al. [23] reported that distance between magnetic ions (jump length 'L') of the electrons affects the fundamental properties in ferrites. The distance between magnetic ions (jump length 'L') for each tetrahedral (A-site) and octahedral (B-site) i.e. 'L_A' and 'L_B' respectively has been calculated from the following relations [24].

$$L_A = \frac{\sqrt{3}}{4} a \tag{4}$$

$$L_B = \frac{\sqrt{2}}{4} a \tag{5}$$

Where, 'a' is the lattice parameter.

Both the jump length 'L_A' and 'L_B' are directly proportional to the lattice parameter 'a'. Hence, it has been observed that both 'L_A' and 'L_B' were found to be decreased with increase in nickel substitution (x) as shown in Table 1.

Magnetic Studies

Magnetizations of the as-prepared samples have been measured using a VSM at room temperature. The hysteresis curves of Mn_{0.5-x}Ni_xZn_{0.5}Fe₂O₄ (x=0.0, 0.1, 0.2, 0.3) ferrite nanoparticles are shown in Fig. 5 and magnetic parameters are presented in Table 2. It has been observed that all the samples exhibited narrow hysteresis loops, with a behavior characteristic of soft magnetic materials [25].

The magnetic moment per formula unit (n_B) in Bohr magneton (μ_B) was calculated by using the following equation [26].

$$n_B = \frac{M_{wt} \times M_s}{5585} \tag{6}$$

Where M_{wt} is the molecular weight of the sample and M_s is the saturation magnetization in the electromagnetic unit.

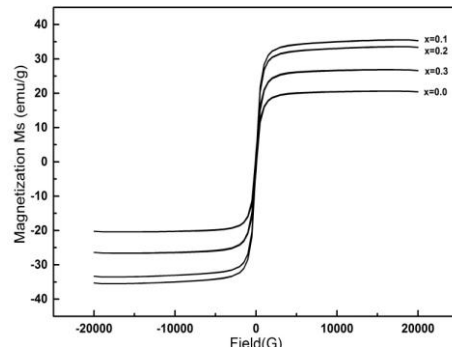


Figure 5: Hysteresis curves of Mn_{0.5-x}Ni_xZn_{0.5}Fe₂O₄ (x=0.0, 0.1, 0.2, 0.3)

Table 2: Observed and reported magnetic parameters of Mn_{0.5-x}Ni_xZn_{0.5}Fe₂O₄ (x=0.0, 0.1, 0.2, 0.3)

X	M _s (emu/g)		H _c (Oe)		M _r (emu/g)		K (erg/Oe)		R (M _r /M _s)		n _B (μ _B)	
	Obs.	Rep. [20]	Obs.	Rep. [20]	Obs.	Rep.	Obs.	Rep.	Obs.	Rep.	Obs.	Rep. [40]
0.0	20.5	14	25.7	0.65	0.90	-	537.60	-	0.044	-	0.864	3.386
0.1	34.2	12	21.2	0.39	1.02	-	739.87	-	0.029	-	1.446	3.382
0.2	32.3	11	40.2	0.29	1.83	-	1325.61	-	0.056	-	1.370	3.381
0.3	26.2	15	76.2	0.19	2.87	-	2038.27	-	0.109	-	1.109	3.449

It has been observed that the magnetization of all the samples increases with increasing applied magnetic field that attains saturation magnetization up to the field 6000 Gauss. Similar observations at room temperature, magnetizations have been reported by C. Venkataraju et al. [20] and K. Jalaiah et al. [27]. It has been also observed that as the Ni ion concentration increases, nickel goes to B-site and transfer Fe³⁺ ions from B-site to the A-site [28]. Thus increase in the magnetization of the A-sublattice is expected. The increasing iron content at A-site results in the A-B interaction gradually increases, as experienced by the B-site iron ions and this reduces the canting of spins of B-site iron ions. Therefore the magnetization of the A-sublattice increases. At the same time, decreased iron contents at B-site reduce the magnetization of the B-sublattice. The net magnetic moment (M) is the sum of the magnetization of A and B-sublattices, i.e. M=M_B-M_A. Hence the net magnetization decreases. The initial increase in magnetization has been observed, which is due to dominant effects of spin canting over the combined effects of increase and decrease of iron ions at A and B sites respectively [29]. However for composition x=0, i.e. for higher Mn²⁺ ion concentrations, more Fe³⁺ ions being at B-site, the increased B-B interaction decreases the magnetization of the B-site. D.R.Mane et al [30] reported magnetic properties to alter significantly due to the formation of Fe₂O₃ as a result of zinc loss. The variation of magnetization with Ni content is shown in Fig. 6.

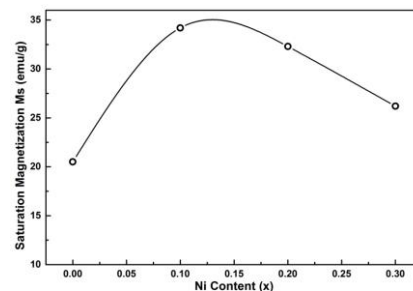


Figure 6: Variation of Saturation Magnetization M_s with Ni content

The Stoner-Wohlfarth model which explained Coercivity value as:

$$H_c = \frac{2K}{\mu_0 \times M_s} \quad (7)$$

Where K is the anisotropy constant, μ_0 is the universal constant of permeability at free space and M_s is the saturation magnetization. According to this model, Coercivity is inversely proportional to the saturation magnetization [31]. The variation of coercivity with Ni content is shown in Fig. 7. For all the substitutions, the Ni^{2+} ions system may be deliberated as hidden. This may interpret the almost linear dependence of K on Ni^{2+} ion concentration. It has been observed that the anisotropy constant (K) increases with increase in Ni^{2+} ion concentration. The anisotropy constant of ferrites is interpreted by the one-ion model. It is also known that the anisotropy field in ferrite nanoparticles results from the presence of Fe^{2+} ions [32]. It is generally recognized that in ferrites, electron exchange between Fe^{2+} and Fe^{3+} ions on B-sites is due to dominant conduction mechanism [33]. Apparently, with an increase in Ni substitution, Fe^{2+} ion concentration increases as a result anisotropy constant (K) increases. The variation of anisotropy constant (K) with Ni content is shown in Fig. 8.

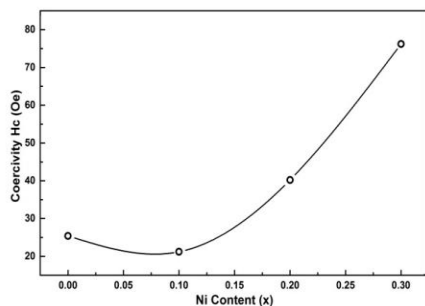


Figure 7: Variation of coercivity ' H_c ' with Ni content

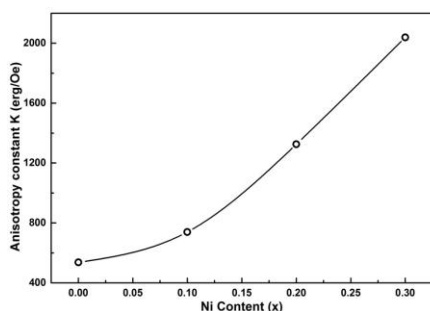


Figure 8: Variation of anisotropy constant ' K ' with Ni content

The remnant ratio $R = M_r/M_s$ is an indication of the ease with which the direction of magnetization reorients to the nearest easy axis magnetization direction after the magnetic field is removed. The values of the remnant ratio of the prepared samples are in the range 0.029 - 0.109. The low value of R is an indication of the isotropic nature of the material [34] and behavior of powder ferrite [35]. It has been observed that the hysteresis curves of the samples are near rectangular in shape which exhibits the potential use of these ferrite nanoparticles for memory applications.

EPR Study

The EPR spectra of as-prepared samples have been recorded by scanning the magnetic induction at 9.1 GHz microwave frequency at room temperature. EPR spectroscopy technique is used to investigate the various magnetic parameters such as resonance linewidth (ΔH_{pp}), Resonance field (B) and Lande's splitting factor (g -value) of $Mn_{0.5-x}Ni_xZn_{0.5}Fe_2O_4$ ferrite nanoparticles and the values are listed in Table 3. All the spectra have been analyzed by using Lorentzian distribution function.

Table 3: Observed and reported EPR parameters of $Mn_{0.5-x}Ni_xZn_{0.5}Fe_2O_4$ ($x=0.0, 0.1, 0.2, 0.3$)

Ni Content (x)	Linewidth (ΔH_{pp}) Gauss		Resonance Field (B) Gauss		g-value	
	Obs.	Rep. [40]	Obs.	Rep. [40]	Obs.	Rep. [40]
0.0	627	537	3140	3341	2.072	2.031
0.1	485	349	3210	3345	2.027	2.030
0.2	464	346	3225	3346	2.017	2.029
0.3	548	394	3155	3280	2.062	2.069

The g -value is a function of the molecular motion, the symmetry of the ions and the paramagnetic properties, which is also a constant of proportionality between the field and frequency. The g -value is calculated by the relation [36].

$$g = h\nu/\beta H \quad (8)$$

Where, h is a Planck's constant, ν is the microwave frequency, β is Bohr magneton and H is the magnetic field at the resonance.

The EPR is important for investigating the magnetic properties of ferrites. The linewidth of EPR signal for any ferrite material generally originated from two sources: (i) magnetic dipole-dipole interactions among particles and (ii) Interparticle superexchange interactions between magnetic ions through oxygen ions. Superexchange interaction becomes stronger when the distance between metallic and oxygen ions are smaller and the angle between these two bonds is nearer to 180° . Linewidth may get broadened or narrowed depending upon the interaction inside the material. The large linewidth and g -value rise due to leading dipole-dipole interactions while the small linewidth and g -value rise due to leading superexchange interactions [37].

The increase in nickel content affects the increase in motion of electrons, which consequence in stronger superexchange interaction amidst cations and oxygen ions which reduces linewidth and g -value [38]. For the substitution $x=0.3$, the broad linewidth and the reduced resonance field estimates can be assigned to surface spin disrupt probably due to anti ferromagnetic interactions among the adjoin spins in the magnetic grains [39].

It has been observed that the resonance field (B) increases with Ni content up to substitution $x=0.2$ and then decreases. The variation of the resonance field (B) with Ni content is shown in Fig. 9. It is also observed that both the linewidth (ΔH_{pp}) and g -value decrease with increasing Ni substitution up to $x=0.2$ and then increase. The variations of the linewidth (ΔH_{pp}) and g -value with Ni content are shown in Fig. 10 & 11, respectively.

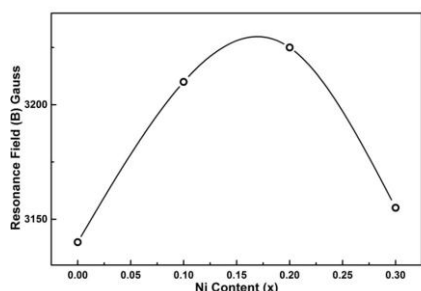


Figure 9: Variation of Resonance Field with Ni content

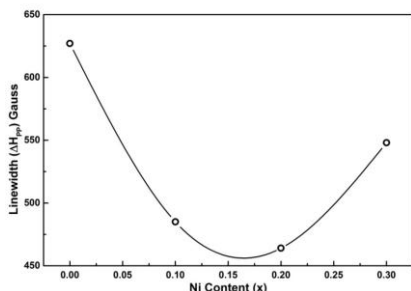


Figure 10: Variation of Linewidth (ΔH_{pp}) with Ni content

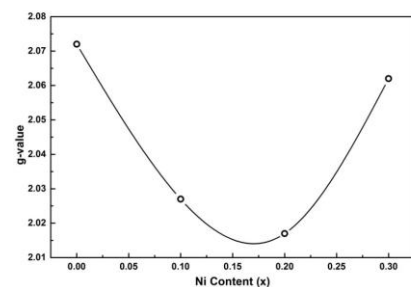


Figure 11: Variation g-values with Ni content

The smaller values of linewidth and g-value in the present work may be due to dominant super exchange interactions between cations and oxygen ions. C. Venkataraju et al. [40] have observed the peak-to-peak linewidth of the EPR spectra of $Mn_{0.5-x}Ni_xZn_{0.5}Fe_2O_4$ ($x=0, 0.1, 0.2, 0.3$) in the range of 537-346 Gauss. It has been observed that the increased peak-to-peak linewidth of the EPR spectra of the samples in the range of 627-464 Gauss is due to the appearance of $\alpha-Fe_2O_3$ [41].

Conclusions

We have investigated structural and magnetic properties of sol-gel prepared $Mn_{0.5-x}Ni_xZn_{0.5}Fe_2O_4$ ($x=0.0, 0.1, 0.2, 0.3$) ferrite nanoparticles. The X-ray diffraction pattern confirms the single-phase ferrite nanoparticles for all the samples. Both crystallite size and lattice parameter have been observed to decrease with increase in nickel substitution. The saturation magnetization is maximum of the sample for $x=0.1$ and then decreases with the increase of nickel substitution. The linewidth and g-value decreases with increase in nickel content up to $x=0.2$ and then increases. This may be due to increase in superexchange interactions among cations and oxygen ions and this can be interpreted by spin-spin and spin-lattice relaxation models. SEM images indicate the morphology of the powders is agglomerated and porous.

Acknowledgements

The Author would like to thank Dr. S. G. Dahotre and, Dr. U. L. Shinde for the co-operation in preparing the samples and IIT Bombay for characterization of the samples.

References

- Chandana Rath, K. K. Sahu, S. D. Kulkarni, S. Anand, S. K. Date, R. P. Das, and N. C. Mishra, Composition dependent particle size and magnetic properties in nanosize $Mn_{1-x}Zn_xFe_2O_4$, ICF 8, Sept.18-Sept.21, 2000, 18 Dp II-4.
- Mohamed Ali Ahmed, Kasim El-Sayed Rady, Kamel Mohamed El-Shokrofy, Ahmed Abo Arais, Mohamed Said Shams, The Influence of Zn^{2+} Ions Substitution on the Microstructure and Transport Properties of Mn-Zn Nanoferrites, Material Sciences and Applications, 2014,5(13),932-942.
- Xuebo Cao and Li Gu, Spindly cobalt ferrite nanocrystals: preparation, characterization and magnetic properties, Nanotechnology, 2005, 16(2), 180-185.
- S. Chikazumi, Physics of Ferromagnetism, Oxford University Press Inc., New York, 1997, Ed 2, 605.
- B. D. Cullity, C. D. Graham, Introduction to Magnetic Materials, John Wiley & Sons Inc., New Jersey, 2009, Ed 2, 176.
- S. Son, M. Taheri, E. Carpenter, V. G. Harris and M. E. McHenry, Synthesis of ferrite and nickel ferrite nanoparticles using radio-frequency thermal plasma torch, Journal of Applied Physics, 2002, 91(10), 7589-7591.
- A. Verma, O. P. Thakur, C. Prakash, T. C. Goel, R. G. Mendiratta, Temperature dependence of electrical properties of nickel-zinc ferrites processed by the citrate precursor technique, Materials Science and Engineering B 116 (2005), 1-6.
- Amarendra K. Singh, T. C. Goel, R. G. Mendiratta, O. P. Thakur and Chandra Prakash, Magnetic properties of Mn-substituted Ni-Zn ferrites, Journal of Applied Physics, 2002, 92(7), 3872-3876.
- Amarendra K. Singh, T. C. Goel and R. G. Mendiratta, Effect of Manganese Impurity on the Conductivity, Dielectric Behaviour and Magnetic Properties of $Ni_{0.3}Mn_xZn_{0.7-x}Fe_2O_4$, Jpn. J. Appl. Phys., 2003, 42, 2690-2691.
- C. O. Ehi-Eromosele, B. I. Ita, E. Ej Iweala, S. A. Adalikwu and P. A. L. Anawe, Magneto-structural properties of Ni-Zn nanoferrites synthesized by the low-temperature auto-combustion method, Bull. Mater. Sci., 2015, 38(5), 1465-1472.
- B. Jeyadevan, C. N. Chinnaamy, K. Shinoda, K. Tohji and H. Oka, Mn-Zn ferrite with higher magnetization for temperature sensitive magnetic fluid, Journal of Applied Physics, 2003, 93(10), 8450-8452.
- N. T. Lan, T. D. Hien, N. P. Duong and D. V. Truong, Magnetic Properties of $Mn_{1-x}Zn_xFe_2O_4$ Ferrite Nanoparticles Prepared by Using Co-Precipitation, Journal of the Korean Physical Society, 2008, 52(5), 1522-1525.
- Jitendra Pal Singh, R. C. Srivastava, H. M. Agrawal, R. P. S. Kushwaha, Prem Chand and Ravi Kumar, EPR Study of Nanostructured Zinc Ferrite, International Journal of Nanoscience, 2008, 7(1), 21-27.
- Manju Kurian, Divya S. Nair, Effect of preparation conditions on Nickel Zinc Ferrite nanoparticles: A comparison between sol-gel auto combustion and co-precipitation methods, Journal of Saudi Chemical Society, 2016, 20, S517-S522.
- C. Venkataraju, R. Paulsingh, EPR studies of Cd-substituted Mn-Zn nanoferrites, International Journal of Nano Dimension, Summer 2015, 6(3), 255-261
- Narinthorn Wiriya, Atipong Bootchanont, Santi Maensiri, Ekaphan Swatsitang, Magnetic properties of $Zn_{1-x}Mn_xFe_2O_4$ nanoparticles prepared by hydrothermal method, Microelectronics Engineering, 2014, 126(c), 1-8.
- Davuluri Venkatesh, G. Himavathi, K. V. Ramesh, Structural, Magnetic, and Electrical Properties of $Ni_{0.65}Zn_{0.35-x}Cu_xFe_2O_4$ Nanoferrite System, J. Supercond Nov Magn, 2015, 28(9), 2801-2807

18. C. Venkataraju, Effect of Nickel on the Structural Properties of Mn Zn Ferrite Nano Particles, Applied Physics Research, 2009, 1(1), 41-45.
19. A. A. Sattar, H. M. El-Sayed, K. M. El-Shokrofy and M. M. El-Tabey, Improvement of the Magnetic Properties of Mn-Ni-Zn Ferrite by the Non-magnetic Al³⁺-Ion Substitution, Journal of Applied Sciences, 2005, 5(1), 162-168.
20. C. Venkataraju, G. Sathish kumar, K. Sivakumar, Effect of cation distribution on the structural and magnetic properties of nickel substituted nanosized Mn-Zn ferrites prepared by co-precipitation method, Journal of Magnetism and Magnetic Materials, 2010, 322(2), 230-233.
21. S. G. Dahotre and L. N. Singh, Study of Magnetic Properties of Nano Structured Mn-Zn Ferrite, Archives of Physics Research, 2011, 2(1), 81-89.
22. M. F. Yan and D. W. Johnson, Jr., Impurity-Induced Exaggerated Grain Growth in Mn-Zn Ferrites, Journal of The American Ceramic Society, 1978, 61(7-8), 342-349.
23. A. Globus, H. Pascard, V. Cagan, DISTANCE BETWEEN MAGNETIC IONS AND FUNDAMENTAL PROPERTIES IN FERRITES, Journal de Physiques, 1977, 38 (C1), C1-163-C1-168.
24. G. Mustafa, M. U. Islam, M. Ahmad, W. Zhang, Y. Jamil, A. W. Anwar, M. Hussain, Investigation of structural and magnetic properties of Ce⁺³ – substituted nanosized Co-Cr ferrites for a variety of applications, Journal of Alloys and Compounds, 2015, 618, 428-436.
25. K. Vijaya Kumar, D. Paramesh, P. Venkat Reddy, Effect of Aluminium Doping on Structural and Magnetic Properties of Ni-Zn Ferrite Nanoparticles, World Journal of Nano Science and Engineering, 2015, 5(4), 68-77.
26. Najmesh Najmoddin, Ali Beitollahi, Huseyin Kavas, Syed Majid Mohseni, Hamidreza Rezaie, John Akerman, Muhammet S. Toprak, XRD cation distribution and magnetic properties of mesoporous Zn-substituted CuFe₂O₄, Ceramic International, 2014, 40(2), 3619-3625.
27. K. Jalaiah, K. Vijaya Babu, Structural, magnetic and electrical properties of nickel doped Mn-Zn spinel ferrite synthesized by sol-gel method, Journal of Magnetism and Magnetic Materials, 2017, 423(1), 275-280.
28. Amrendra K. Singh, T. C. Goel, R. G. Mendiratta, Effect of cation distribution on the properties of Mn_{0.2}Zn_xNi_{0.82x}Fe₂O₄, Solid State Communications, 2003, 125(2), 121-125.
29. Amarendra K. Singh, Abhishek K. Singh, T. C. Goel, R. G. Mendiratta, High performance Ni-substituted Mn-Zn ferrites processed by soft chemical technique, Journal of Magnetism and Magnetic Materials, 2004, 281, 276-280.
30. Dhanraj R. Mane, Damodar D. Birajdar, Sagar E. Shirsath, Raghavender A. Telugu, and Ram. H. Kadam, Structural and Magnetic characterizations of Mn-Ni-Zn ferrite nanoparticles, Phys. Status Solidi A, 2010, 207(10), 2355-2363.
31. Gholam Reza Mirshekari, Shiva Sadat Dae, Hossein Mohseni, SimaTorkian, MehriGhasemi, MoosaAmeriannejad, MoloodHoseinizade, Mohammad pirnia, DanialPourjafar, Maryam Pourmahdavi, KhalilollahGheisari, Structure and Magnetic Properties of Mn-Zn Ferrite Synthesized by Glycine-Nitrate Auto-Combustion Process, Advanced Materials Research, 2012, 409, 520-525.
32. S. Chikazumi, Physics of Ferromagnetism, Oxford University Press Inc., New York, 1997, Ed 2, 288.
33. E. Rezlescu, L. Sachelarie, P. D. Popa, and N. Rezlescu, Effect of Substitution of Divalent Ions on the Electrical and Magnetic Properties of Ni-Zn-Me Ferrites, IEEE Transactions on Magnetics, 2000, 36(6), 3962-3967.
34. Sheena Xavier, Smitha Tankachan, Binu P. Jacob, E. M. Mohammed, Effect of Sintering Temperature on the Structural and Magnetic Properties of Cobalt Ferrite Nanoparticles, Nanosystem: Physics, Chemistry, Mathematics, 2013, 4(3), 430-437.
35. Binod B. Dora, Sanjay Kumar, R. K. Kotnala, Binod Chandra Raula, Mahesh C Sahu, Improved Magnetic Properties of Ni-Zn Nano Ferrites by Using Aloe vera Extract Solution, Int. J. Pharma. Sci. Rev. Res., 2015, 30(1), 294-298.
36. Kisan Zipare, Jyoti Dhumal, Sushil Bandgar, Vikas Mathe, Guruling Shahane, Superparamagnetic Manganese Ferrite Nanoparticles: Synthesis and Magnetic Properties, Journal of Nanoscience and Nanoengineering, 2015, 1(3), 178-182.
37. Jitendra Pal Singh, Gagan Dixit, R. C. Srivastava, Hemant Kumar, H.M.Agrawal and Prem Chand, Magnetic resonance in superparamagnetic zinc ferrite, Bull. Mater. Sci, 2013, 36(4), 751-754.
38. G. S. Shahane, Ashok Kumar, Manju Arora, R. P. Pant, Krishan Lal, Synthesis and characterization of Ni-Zn ferrite nanoparticles, Journal of Magnetism and Magnetic Materials, 2010, 322(8), 1015-1019.
39. Y. Koseoglu, O. Burucu, M. Kumru, F. Yildiz, M. U. Rana, B. Aktas, ESR studies on NiFe₂O₄ ferrites, Proceedings of the Third Moscow International Symposium on Magnetism, 2005, 261-264.
40. C. Venkataraju and R. Paulsingh, FTIR and EPR Studies of Nickel Substituted Nanostructured Mn Zn Ferrite, Journal of Nanoscience, 2014, 1-5. <http://dx.doi.org/10.1155/2014/815385>
41. Shauna Robbenmolt, Stephen S. Sasaki, Tylisia Wallace, Marquise Bartholomew, Sarah H. Tolbert, Fabrication and magnetic properties of Sol-Gel derived NiZn ferrite thin films for microwave applications, Advanced Materials Letters, 2018, 9(5), 345-352.

